Cell Transplantation
2019, Vol. 28(6) 723–738

DOI: 10.1177/0963689718817219
journals.sagepub.com/home/cll
SAGE

Detrimental Role of miRNA-144-3p in Intracerebral Hemorrhage Induced Secondary Brain Injury is Mediated by Formyl Peptide Receptor 2 Downregulation Both *In Vivo* and *In Vitro*

Weijian Fan[1,2], Xiang Li[1], Dongping Zhang[1], Haiying Li[1], Haitao Shen[1], Yizhi Liu[1], and Gang Chen[1]

Abstract

Although microRNA-144-3p (miRNA-144-3p) has been shown to suppress tumor proliferation and invasion, its function in intracerebral hemorrhage (ICH)-induced secondary brain injury (SBI) remains unclear. Thus, this study was designed to investigate the role of miRNA-144-3p in ICH. To accomplish this, we used adult male Sprague-Dawley rats to establish an *in vivo* ICH model by injecting autologous blood, while cultured primary rat cortical neurons were exposed to oxyhemoglobin (OxyHb) to mimic ICH *in vitro*. To examine the role of miRNA-144-3p in ICH-induced SBI, we used an miRNA-144-3p mimic and inhibitor both *in vivo* and *in vitro*. Following ICH induction, we found miRNA-144-3p expression to increase. Additionally, we predicted the formyl peptide receptor 2 (FPR2) to be a potential miRNA-144-3p target, which we validated experimentally, with FPR2 expression downregulated when miRNA-144-3p was upregulated. Furthermore, elevated miRNA-144-3p levels aggravated brain edema and neurobehavioral disorders and induced neuronal apoptosis via the downregulation of FPR2 both *in vivo* and *in vitro*. We suspected that these beneficial effects provided by FPR2 were associated with the PI3K/AKT pathway. We validated this finding by overexpressing FPR2 while inhibiting PI3K/AKT *in vitro* and *in vivo*. In conclusion, miRNA-144-3p aggravated ICH-induced SBI by targeting and downregulating FPR2, thereby contributing to neurological dysfunction and neural apoptosis via PI3K/AKT pathway activation. These findings suggest that inhibiting miRNA-144-3p may offer an effective approach to attenuating brain damage incurred after ICH and a potential therapy to improve ICH-induced SBI.

Keywords

intracerebral hemorrhage, microRNA-144-3p, formyl peptide receptor 2, apoptosis

Introduction

Cerebral hemorrhage, which accounts for approximately 50% of mortalities and morbidities, has different subtypes, including intracerebral hemorrhage (ICH), which are triggered by small vessel ruptures deep within the brain parenchyma[1]. Furthermore, of the patients who survive, 75% suffer from varying degrees of damage to motor, sensory, mind-set, and other irreplaceable brain functions. Even when combining complex remedies, secondary brain injury (SBI) can occur following ICH and disappointing prognoses are inevitable[2,3]. For many decades, medical research has been devoted to uncovering an effective and direct remedy to attenuate SBI and improve the neurological outcomes following ICH[4–6]. Until now, however, no clinical treatment has been found to offer any significant long-term improvements when facing ICH-induced SBI and its associated pathologies, such as edema, inflammation, neurological dysfunction, neuron degeneration, and even hernia[7,8].

[1] Department of Neurosurgery, Brain and Nerve Research Laboratory, The First Affiliated Hospital of Soochow University, Suzhou, China
[2] Department of Vascular Surgery, Suzhou Hospital Affiliated of Nanjing Traditional Chinese Medicine University, Suzhou, China

Submitted: June 1, 2018. Revised: October 30, 2018. Accepted: November 13, 2018.

Corresponding Authors:
Gang Chen and Yizhi Liu, Department of Neurosurgery, Brain and Nerve Research Laboratory, The First Affiliated Hospital of Soochow University, 188 Shizi Street, Suzhou 215006, China.
Email: nju_neurosurgery@163.com

Brain tissues can respond to ICH via extremely intricate mechanisms, sometimes involving microRNAs (miRNAs). These miRNAs are evolutionarily conserved, endogenous, noncoding RNAs that regulate both transcriptional and posttranscriptional gene expression by binding mRNA transcripts or by binding to the 3′-untranslated region (3′-UTR) of a target to ultimately prevent protein synthesis[9]. Moreover, miRNAs have been identified in a large variety of cell types and found to participate in a multitude of physiological processes, including cell proliferation, cell migration and invasion, disease prognosis, biological secretin production, stroke, tumorigenesis, and cancer pathology[10,11].

Of specific interest is miRNA-144-3p, which belongs to the miR-144/451 cluster and miR-144 family. Recent studies have shown that miRNA-144-3p is a critical factor in tumorigenicity, with the ability to induce or suppress tumor growth by acting as an oncogene or inhibitor; these behaviors typically are seen in hepatocellular carcinoma, lung cancer, thyroid cancer, or renal cell carcinomas[8,12–14]. Furthermore, miRNA-144-3p has been reported recently to have several targets. For instance, in hepatocellular carcinomas, miRNA-144-3p targets SGK3 and suppresses tumor growth and angiogenesis; in gastric cancer, it targets PBX3 and inhibits progression; and in multiple myeloma, it targets c-Met and restrains cell proliferation[15,16]. Moreover, in non-small-cell lung cancer (NSCLC), miRNA-144-3p has been shown to inhibit tumor growth and induce apoptosis by directly modulating ZFX expression[17]. Additionally, in prostate cancer cells, miRNA-144-3p suppression via cisplatin-induced vascular endothelial growth factor induces autophagic cell survival because of an upregulation of beclin-1[18]. Furthermore, miRNA-144 has been reported to induce microglial autophagy and inflammation following ICH, with downregulation of miRNA-144 improving neurological functions[19]. Moreover, studies have suggested that miRNA-144-3p suppression can attenuate oxygen–glucose deprivation/reoxygenation-induced neuronal injury by promoting Brg1/Nrf2/ARE signaling[20]. Therefore, we surmised that miRNA-144-3p may play a similar role during ICH induction. Recent findings have shown that miRNAs are widely associated with cerebral physiological and pathological processes, and that in neurons, miRNAs are cleared by the Drosha ribonuclease III enzyme and transported to the cytoplasm where mature miRNAs are generated by Dicer ribonuclease[21].

One protein that has been associated with hemorrhage is formyl peptide receptor type 2 (FPR2), which was found to be an miRNA-144-3p target herein[22]. FPR2, also known as ALX (lipoxin A4 receptor), is considered to be a special G-protein-coupled receptor that has the ability to transduce physiological and pathological information produced by proteins, peptides, and lipid ligands[23]. Furthermore, FPR2 is believed to play a critical role in anti-inflammatory and pro-resolution processes, especially by promoting macrophage clearance and inhibiting metalloproteinase activation[23,24]. Moreover, in endothelial cells and myeloid lineages, FPR2 has been shown to modulate neutrophil apoptosis and macrophage efferocytosis through ligand-affinity binding[25]. FPR family members have been characterized in a large variety of experimental animal models, including stroke, subarachnoid hemorrhage (SAH), trauma, and anticancer processes[22,26–28]. Moreover, FPR2 has been shown to play a double-sided role in stroke and SAH via a traditional PI3K/AKT signal transduction pathway[29,30]. However, the activation of FPR2 in neurons and the similar or opposite functions it may perform in ICH, as well as in SBI or other cerebral pathologies, remains elusive. This study focused on the effect of miRNA-144-3p during ICH induction and its potential mechanisms and also determined whether miRNA-144-3p could target FPR2 and suppress its function as a means of neural protection.

Materials and Methods

Experimental Animals

All animal experimentation was approved by the Institutional Animal Care Committee of Soochow University (Suzhou, Jiangsu, China) and was compliant with the Animal Research: Reporting *In Vivo* Experiments (ARRIVE) guidelines. Nearly 200 adult male Sprague-Dawley (SD) rats weighing 250–300 g were purchased from the Shanghai Experimental Animal Center (Shanghai, China). All rats were housed in a quiet environment at a constant temperature and humidity and with a 12 h light/dark cycle. Food and water were freely available.

Establishing an ICH Model

Adult male SD rats were anesthetized with 4% chloral hydrate via intraperitoneal injection at a dosage of 1 ml per 100 g. After completing anesthesia, the rats were fastened in a stereotactic apparatus frame (Shanghai Ruanlong Science and Technology Development Co., Ltd., Shanghai, China). The injection site was precisely positioned above the basal ganglia, with access gained using a bone drill positioned about 3 mm lateral to the bregma. Next, 100 μl of autologous blood was collected from the heart using a 100 μl microinjector (Hamilton Company, Reno, NV, USA) and injected through the burr hole into the corpus striatum using a microsyringe. The overall injection procedure lasted 5 min and the depth of puncture was approximately 5.5 mm. A sham control group was generated by performing the same procedure, but by replacing the autologous blood with an equal volume of physiological saline solution. Bone wax was then utilized to prevent cerebrospinal fluid (CSF) and blood leakage. Representative ICH brain samples are shown in Fig. 1A.

Primary Neuron Cultures and an In Vitro ICH Model

First, we extracted 17-day-old rat embryos and removed their brains. Blood vessels and meninges were removed at 4°C under a microscope, and then the brain samples were

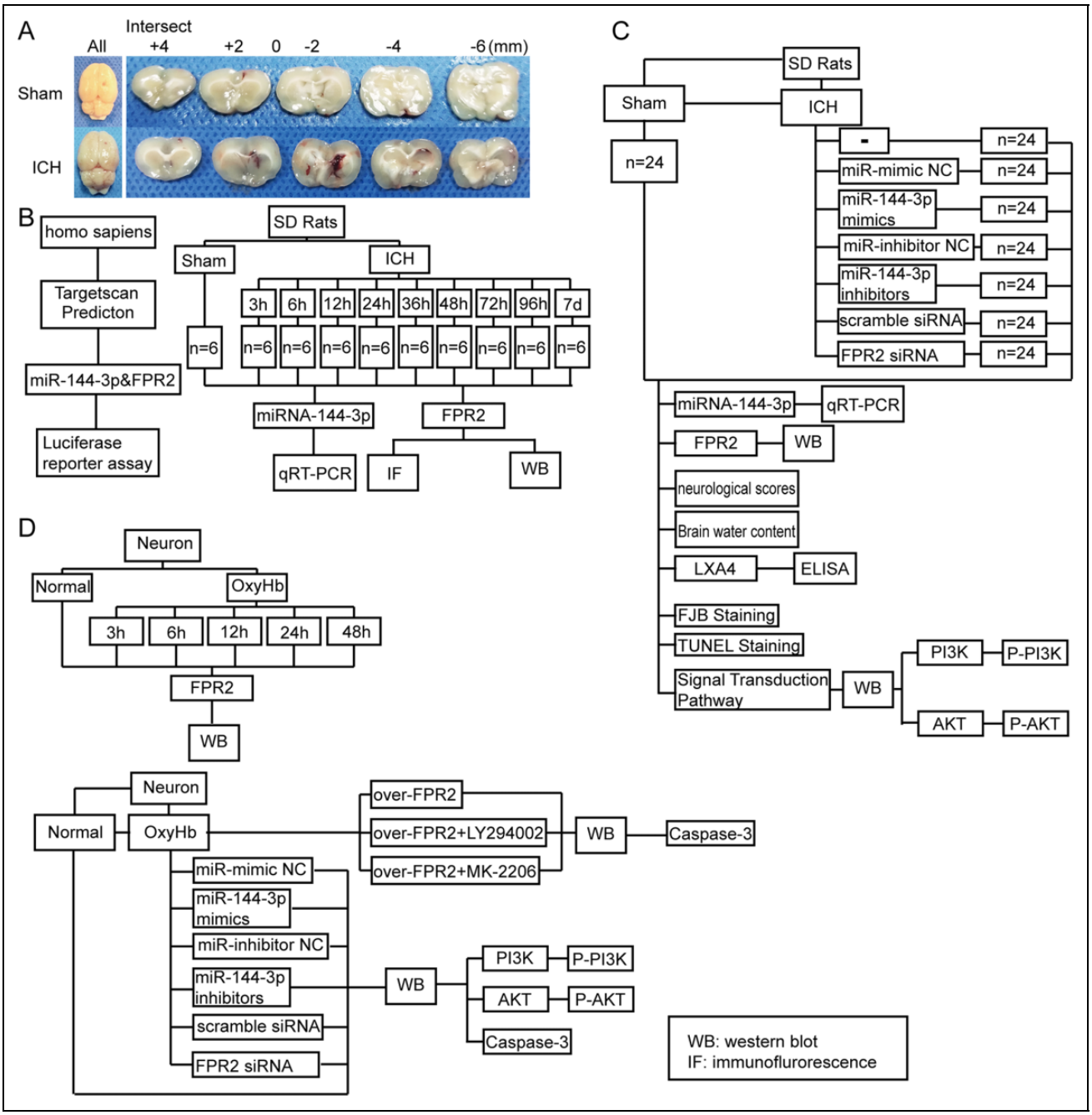

Fig. 1. Establishments of an ICH model and experimental flow map. (A) Representative images of brain cortical tissues with a hematoma after infusion with autologous blood or with saline for the sham group. (B) Luciferase report between formyl peptide receptor 2 (FPR2) and miRNA-144-3p in 293 T cells. Time-courses examining miRNA-144-3p and FPR2 expression in brain perihematoma regions. (C and D) The role of miRNA-144-3p in regulating FPR2 after ICH-induced secondary brain injury (SBI) and its potential mechanisms.

trypsin digested for 5 min and centrifuged (500× g, 5 min). We cultured the obtained cortical neurons in six-well plates with neurobasal medium (GIBCO; Carlsbad, CA, USA) in an incubator at 37°C and 5% CO_2. Half of the medium was refreshed every 2 d and the neuron morphology and activity was microscopically observed. To simulate ICH in the brain, we exposed the fostered neurons to 10 μM oxyhemoglobin (OxyHb; Ruibio, O7109).

Experimental Grouping

Part I: time-course analysis of miRNA-144-3p expression and FPR2 protein expression after ICH in vivo *and their connection.* We used a luciferase reporter analysis to examine the relationship between miRNA-144-3p and FPR2 protein expression in the 293 T cell line. In *in vivo* experiments, we randomly divided 66 rats (we used 70 rats, but only 66 rats

survived after ICH model establishment) into 11 groups (6 rats per group), a normal group, a sham group, and 9 experimental groups harvested at 3 h, 6 h, 12 h, 24 h, 36 h, 48 h, 72 h, 96 h, and 1 w post-ICH induction. For each group, we extracted brain cortexes ($n = 6$) for real-time polymerase chain reaction (PCR), Western blot analysis, and double immunofluorescence analysis (Fig. 1B).

Part II: role of miRNA-144-3p in ICH-induced SBI and its underlying mechanisms in vivo. We randomly divided the rats into 8 groups ($n = 24$ per group): a sham group, ICH group, ICH + miRNA-144-3p mimic group (negative control), ICH + miRNA-144-3p mimic group, ICH + miRNA-144-3p inhibitor group (negative control), ICH + miRNA-144-3p inhibitor group, ICH + control siRNA group, and ICH + FPR2 siRNA group. At 24 h post-ICH induction, we extracted brain tissues as described earlier and analyzed the tissue via Western blot, real-time PCR, terminal deoxynucleotidyl transferase-mediated dUTP nick-end labeling (TUNEL), and Fluoro-Jade B (FJB) staining. In addition, we subjected 6 rats per group to a brain edema evaluation, and examined 12 rats per group for behavioral impairment at 1 w post-ICH induction (Fig. 1C). We also extracted and examined CSF using an enzyme-linked immunosorbent assay (ELISA). Furthermore, we obtained the tissue samples utilized for Western blot analysis 1 mm away from the hematoma to avoid potential red blood cell contamination.

Part III: time-course analysis of FPR2 protein expression in vitro, miRNA-144-3p functions during ICH-induced SBI and latent signal transduction pathways in vitro. We divided the obtained primary neurons into a control group and 5 experimental groups (Fig. 1D), with samples obtained at 3 h, 6 h, 12 h, 24 h, and 36 for Western blot analysis. The cultured neuron groups included a control group, OxyHb group, OxyHb + miRNA-144-3p mimic group (negative control), OxyHb + miRNA-144-3p mimic group, OxyHb + miRNA-144-3p inhibitor group (negative control), and OxyHb + miRNA-144-3p inhibitor group. At 12 h post-OxyHb treatment, we collected the neurons for Western blot analysis.

Antibodies

Antibodies obtained from Abcam (Cambridge, MA, USA) included anti-PI3 K (ab191606), anti-p-PI3 K (ab162651), anti-AKT (ab179463), anti-p-AKT (ab131443), and anti-NeuN antibody-neuronal cell marker (ab104224; FOX3). Antibodies purchased from Cell Signaling Technology (Danvers, MA, USA) included anti-caspase-3 (9661), and those purchased from Santa Cruz Biotechnology (Santa Cruz, CA, USA) included β-tubulin (sc-9140) and β-actin (sc-8227) and secondary goat anti-rabbit IgG-HRP (sc-2004) and goat anti-mouse IgG-HRP (sc-2005) antibodies used for Western blotting. Antibodies from Invitrogen (Carlsbad, CA, USA) included secondary Alexa Fluor-488 donkey anti-rabbit IgG (A21206), Alexa Fluor-555 donkey anti-mouse IgG (A31570), and Alexa Fluor-555 donkey anti-rabbit IgG (A31572) antibodies used for immunofluorescence.

Western Blot

We collected the unilateral cortex of the brain from rats at 24 h post-ICH induction as previously described[26]. Briefly, for each group, we loaded 50 μg of protein sample per lane. After electrophoresis, we transferred the proteins to polyvinylidene difluoride membranes, which were then blocked with 5% nonfat milk for 2 h at 37°C. The membranes were then incubated with primary antibodies, followed by incubating with horseradish peroxidase-labeled secondary antibodies and imaged. We analyzed the obtained images using the Image J program.

Real-Time PCR

To precisely quantify miRNA-144-3p expression, we performed real-time PCR. We extracted RNA from the brain tissues using TRIzol reagent (Invitrogen Life Technologies, Carlsbad, CA, USA) according to the manufacturer's instructions. Real-time PCR was performed using a Rever-Tra Ace® qPCR RT kit (FSQ 101; Toyobo, Osaka, Japan) and then the miRNA was reverse transcribed using a First Strand cDNA Synthesis kit. Real-time PCR reactions were visualized using SYBR® qPCR Mix (QPS 201, Toyobo) as previously described[15]. Samples were normalized to sham group and glyceraldehyde 3-phosphate dehydrogenase expression levels and the miRNA-144-3p primers included miRNA-144-3p forward (5′-GGCGTACAGTATAGATGAT-3′) and reverse (5′-GAGCAGGCTGGAGAA-3′) primers. We calculated the fold changes using the comparative computed tomography (CT) method ($2\Delta\Delta Ct$), with all reagents, apparatuses, and procedural protocols being the same as those described previously[31].

Examining the Function of miRNA-144-3p Using an miRNA Mimic and siRNA

To evaluate the function of miRNA-144-3p, its mimics and an inhibitor were purchased from RiboBio Co., Ltd. (Guangzhou, China). Also, to knock down the membrane protein FPR2, silencing RNA (siRNA) was obtained (RiboBio Co., Ltd.). Following transfection *in vitro*, we determined the knockdown efficiencies of these siRNAs using Western blotting. The FPR2 siRNA target sequences included (1) CCAGTGATACAGGCACAAA, (2) GAAGTGCTGGACGTAGCAA, and (3) ACGGAATTCTTAAGATGTG, and we used only those sequence with the highest efficacy.

Luciferase Reporter Analysis

To determine if a connection exists between miRNA-144-3p and FPR2 and if they combine at the 3′-UTR, we used TargetScan (www.targetscan.com) and MicroRNA (www.microrna.org). After completing the prediction, we performed a dual luciferase reporter assay. We synthesized a Has-FPR2-3′-UTR-mutant using PCR site-directed mutagenesis, with the ATACTGT sequence (647–653) within the 3′-UTR of the target gene replaced with TATGACA. The wild type and mutant type were then cloned into a site downstream of the luciferase reporter gene within the pMIR-Report vector (Promega, Madison, WI, USA). We cultured HEK293 T cells in 96-well plates in 100 µl per well and incubated the cells at 37°C for 24 h. Each well was then transfected with a combination of miRNA-144-3p mimics, non-target control, reporter plasmid, or mutant plasmid and Lipofectamine 3000 (Invitrogen, Carlsbad, CA, USA). Afterward, firefly and renilla luciferase activities were measured using a Dual-Glo® Luciferase Assay System (Promega), with hRluc used as the fluorescence reporter and hluc used as an internal reference. Relative Rluc/luc ratios were determined and visualized in bar graphs using GraphPad Prism[32].

Immunofluorescence Analysis

We collected rat brain tissues and immersed the samples in 4% paraformaldehyde and embedded in paraffin. Each sample was sliced into 10 sections, fixed onto a glass slide, and stored under lucifugal and desiccative conditions before staining. Normal rabbit immunoglobulin G (IgG) and normal mouse IgG were used as negative controls and were introduced in addition to the immunofluorescent antibodies. We observed the images and recorded them using a fluorescent microscope (Olympus BX50/BX-FLA/DP70; Olympus Co., Japan) and analyzed the relative intensities using Image J software (National Institutes of Health, Bethesda, MD, USA).

TUNEL and FJB Staining

To examine neural apoptosis and degeneration within the samples, we performed TUNEL and FJB staining as previously described[33]. Briefly, we obtained the samples as described and sliced the paraffin-embedded brain samples sliced into 4 µm sections. For TUNEL staining, we used an In Situ Cell Death Detection kit (Roche, 11684795910) according to the manufacturer's protocols. For FJB staining, all of the reagents, such as NaOH, KMnO4, ethyl alcohol, acetic acid, and phosphate buffered saline (PBS), were purchased from Hushi reagents (Shanghai Hushi laboratorial Equipment Co., Ltd, Shanghai, China). To optimize pigmentation and coloration when using the FJB solution, we incubated samples in the dark for at least 20 min. We observed both TUNEL and FJB stained sections under a fluorescence microscope (Olympus BX50/BX-FLA/DP70; Olympus Co.) and analyzed the sections using Image J software.

Brain Edema

We used a core estimation method to determine the volume of water content in the brain as previously described[34]. Briefly, rats were anesthetized and beheaded without cardiovascular lavage. We divided the brains into five regions: the contralateral substantia medullaris, contralateral cortex, ipsilateral substantia medullaris, ipsilateral cortex, and cerebellum. We determined and recorded wet weights after removal. The tissues were then incubated in a microwave oven at 105°C for at least 24 h to allow for desiccation, and then we obtained a dry weight. The formula for determining the percentage of water content was as follows: [(wet weight – dry weight)/wet weight] × 100%.

ELISA

We evaluated the quantitative volume of Lipoxin A4 (LXA4) using ELISA as described previously[22]. Artery blood was extracted and centrifuged for 10 min and serum was collected for further analysis. LXA4 conjugated horseradish peroxidase (HRP) was added and allowed to incubate at 37°C for 30 min. TMB substrate solution was then added to each well and allowed to incubate in the dark for 15–20 mins. Next, we used a stop buffer to terminate the reaction and measured the absorbance spectrophotometrically at 450 nm using an iMark microplate reader (Bio-Rad, Hercules, CA, USA). Finally, we analyzed the obtained data using GraphPad Prism software.

Neurological Improvements

We included at least 6 rats from each group in the neurological evaluation. The time range for observation was 14 days and we conducted the procedures as previously described[35,36]. Three aspects were examined, including activity, appetite, and deficits, to obtain a comprehensive assessment of the neurological deficits that were acquired after ICH. The score range was from 0 to 2, with 2 being the worst, and 0 representing sanity, respectively. The total minimum score was 0 and maximum was 6.

MiRNA and siRNA Transfections in Rats and Neurons

We performed transfection of the miRNA-144-3p mimic and inhibitor and the FPR2 siRNA using Entranster-*in vivo* RNA transfection reagent (18668-11-1; Engreen, Beijing, China), with dilutions prepared in DEPC RNase-free water. At 48 h prior to the establishment of an ICH model, we injected the solution intracerebroventricularly using the procedures described by Senn et al[37].

For *in vitro* experiments, we performed transfections using Lipofectamine® 3000 Transfection Reagent (L3000-015; Invitrogen, Carlsbad, CA, USA) according to the

manufacturer's instructions. At 48 h post-transfection, we mixed the cultivated neurons with OxyHb for a certain number of hours before cell harvesting.

Flow Cytometry

We combined the cultured neurons, which were divided into different experimental groups, with 0.25% trypsin (without EDTA) and centrifuged at 300× g for at least 5 min. We then removed the supernatants and resuspended the remaining pellets in 500 μl of binding buffer. Next, we mixed the samples with 3 μl annexin V and 2.5 μl PI (Beyotime, China) to add pigmentation and incubated the samples for 20 min in the dark at 37°C. We analyzed each tube by flow cytometry (FACS Calibur, BD Biosciences, USA) and recorded more than 20,000 events per sample. The obtained images were recorded and analyzed as previously described[38].

Statistical Analysis

We expressed all data as a mean ± SEM. We analyzed statistical variations using a Student's *t* test and to do comparisons between two groups. When comparing more than two groups, we utilized a one-way analysis of variance (ANOVA). We presented neurobehavioral scoring as a median with an interquartile range. Findings were considered statistically significant if $P < 0.05$ was obtained and all experimental data were analyzed using GraphPad Prism 7.00.

We performed post-hoc power analysis using PRISM with a *t* test comparison of the means. A two-sample *t* test was performed with a mean difference between the sham and ICH groups ($n = 6$ per group) determined, with an estimated standard deviation, $\alpha = 0.05$, and power > 0.75. We assigned 6 rats to each group because this number was closest to the prediction.

Results

MiRNA-144-3p Levels Were elevated After ICH Induction

The levels of miRNA-144-3p in the perihematomal region of the brain after ICH induction were quantified using real-time PCR. The results illustrated that the relative miRNA-144-3p levels were significantly upregulated by 12 h post-ICH induction, with levels peaking at 24 h and then slowly decreasing from there onward (Fig. 2A).

FPR2 Predicted as an miRNA-144-3p Target

To identify if FPR2 is a potential miRNA-144-3p target, we used the TargetScan software and identified two poorly conserved miRNA-144-3p binding sites located in the 3′-UTR of FPR2 at positions 647–653 and 1520–1526. To explore whether miRNA-144-3p can strongly associate with FPR2, we cloned both a 3′-UTR wild type and mutant into a luciferase reporter vector. The results showed that miRNA-144-3p significantly reduces the luciferase activity when binding with the wild type 3′-UTR, but no obvious effect was noted in the presence of the mutant (Fig. 2B).

FPR2 Expression was Downregulated by miRNA-144-3p after ICH Induction

To further determine brain FPR2 protein levels around a hematoma, we classified all of the samples by time shaft and analyzed the samples by Western blotting. The results showed that the FPR2 protein levels reduced gradually, starting at 3 h post-ICH induction, with the lowest levels reached at 24 h. Thus, a corresponding trend would be expected in the miRNA-144-3p expression (Fig. 2C). Moreover, we further evaluated FPR2 levels by immunofluorescence staining with neuronal nuclei, a specific neuron marker, and the images revealed that neuron FPR2 levels were reduced at 24 h post-ICH induction when compared with the sham group (Fig. 2D).

MiRNA-144-3p Aggravates Neuron Degeneration and Apoptosis and Deteriorates Neurological Outcomes

To further examine the association between miRNA-144-3p and FPR2, we infused a miRNA-144-3p mimic and inhibitor cerebroventricularly and determined miRNA levels using real-time PCR. The miRNA-144-3p levels increased markedly in the mimic group, while showing a partial decrease in the inhibitor group (Fig. 3A). It is well known that LXA4 is a common lipoxin with a strong affinity for the FPR2 receptor, and thus it was also examined. Within the CSF, the LXA4 levels were affected by the mimic and inhibitor before ICH and at 24 h post-ICH induction as determined by ELISA. The results showed that LXA4 levels decreased markedly after ICH, with an even further decrease seen in the presence of the mimic or siRNA group, but with a bit of an increase seen in the presence of the inhibitor (Fig. 3B). Additionally, we detected brain FPR2 expression at 24 h post-ICH induction by Western blotting, which showed that the injection of the miRNA-144-3p mimic decreased FRP2, whereas the inhibitor and siRNA increased FPR2 expression (Fig. 3C). These results suggest that FPR2 is an miRNA-144-3p target.

After administering the miRNA-144-3p mimic and inhibitor and the FPR2 siRNA, we measured brain water content at 24 h post-ICH induction, and determined neurological scores at 1 w post-ICH induction. Both the miRNA-144-3p mimic and the FPR2 siRNA were found to increase the brain water percentage and minimize the neurological scores, whereas the inhibitor attenuated cerebral edema and improved the neurological scores (Figs. 3D and 3E).

To more deeply explore the function of miRNA-144-3p in an ICH model, we performed FJB staining to detect the degree of neuronal degeneration. In the presence of the miRNA-144-3p mimic, the density of FJB-positive cells was

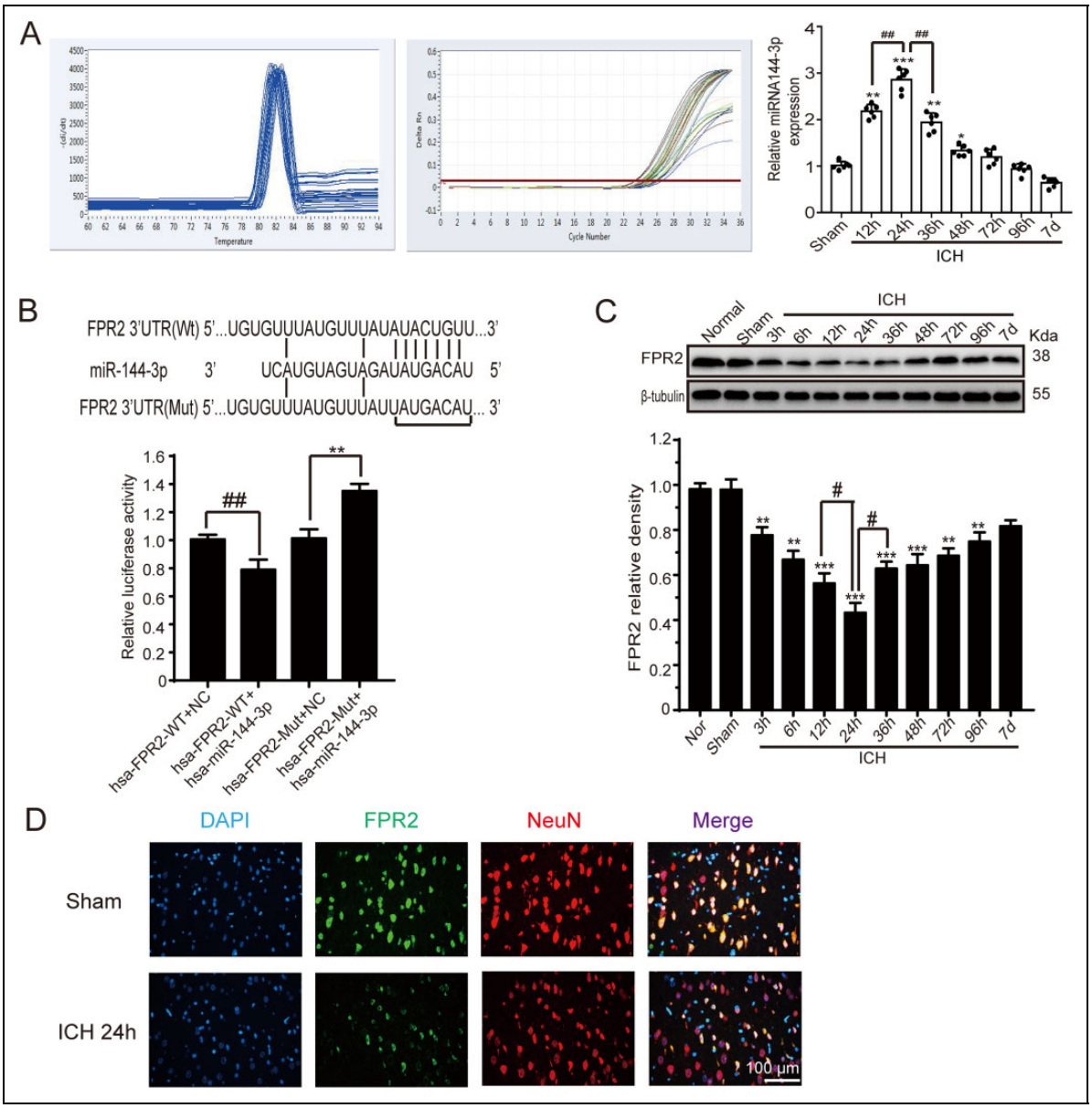

Fig. 2. MiRNA-144-3p and FPR2 expression after ICH. Adult male Sprague-Dawley (SD) rats were induced with ICH and brain samples were collected at various time points. (A) Real-time PCR analysis of miRNA-144-3p expression in perihematoma regions and the associated capacity curve. (B) Luciferase reporter analysis examining miRNA-144-3p and an FPR2 with a mutant or wild type 3′-UTR. (C) Western blot analysis and quantification of FPR2 levels in brain tissue collected in proximity to the hematoma at various time points. (D) Immunofluorescent staining of brain sections from the sham and ICH groups, with anti-FPR2 antibody (green), anti-NeuN antibody (red), and DAPI (blue) staining. Representative sham and ICH images at 24 h. All mean values for the sham group were normalized to 1.0 and all data are shown as a mean $\pm$ SEM. *P < 0.05, **P < 0.01, and ***P < 0.001 vs. sham group; $^{\#}$P < 0.05, $^{\#\#}$P < 0.01, and $^{@}$ P < 0.05 as indicated in the figure; $n = 6$.

shown to increase, whereas the miRNA-144-3P inhibitor alleviated the ICH-induced damage when compared with the ICH control group (Figs. 4A and 4B). Furthermore, we performed double immunofluorescent staining using TUNEL and NeuN. The images showed that the sham group had only a small number of TUNEL-positive neurons, whereas the ICH group showed an increase in the number of apoptotic neurons (Figs. 4C and 4D). Moreover, the proportion of apoptotic cells was significantly higher in the presence of the miRNA-144-3p mimic and substantially lower with the inhibitor (Figs. 4C and 4D).

Neuronal Protective Effect of FPR2 is Induced by the PI3K/AKT Pathway and is Reversed by miRNA-144-3p upregulation In Vivo

Various studies have reported that FPR2 can have a rescue effect in various situations, with some studies suggesting that

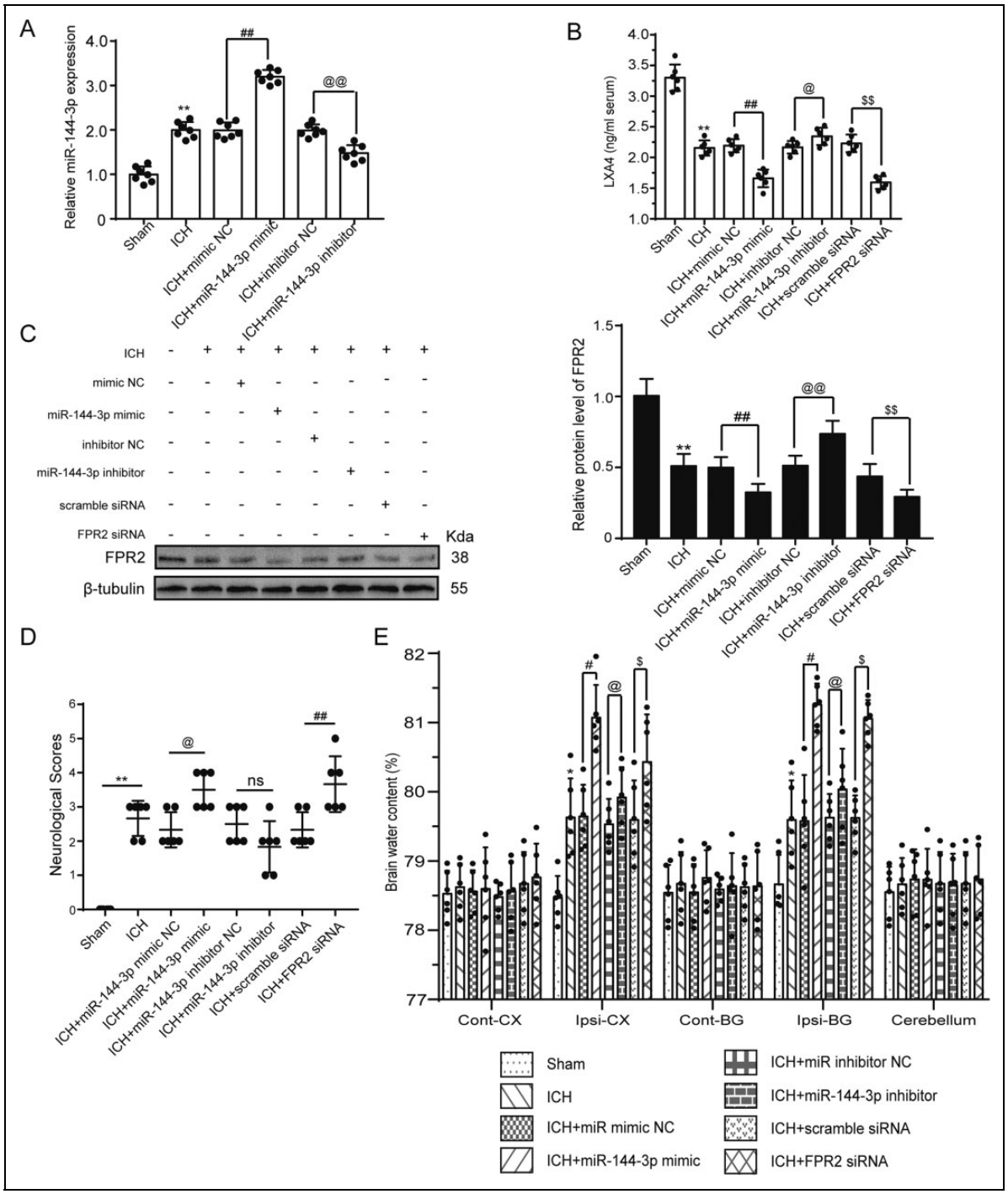

Fig. 3. MiRNA-144-3p downregulated FPR2 expression and induced neurological deficits and brain edema. Rats were randomly divided into 8 groups ($n = 24$ per group): sham group, ICH group, ICH + miRNA-144-3p mimic group (negative control), ICH + miRNA-144-3p mimic group, ICH + miRNA-144-3p inhibitor group (negative control), ICH + miRNA-144-3p inhibitor group, ICH + control siRNA group, and ICH + FPR2 siRNA group. All vectors, siRNA or miRNAs, were transfected 48 h before ICH induction and then brain samples were collected. (A) Real-time quantification of miRNA-144-3p expression after utilizing an miRNA-144-3p mimic or inhibitor. (B) LXA4 quantification in CSF within these groups as determined by ELISA. (C) Western blot analysis of brain FPR2 levels following miRNA-144-3p mimic or inhibitor transfection, after ICH induction, when compared with the control group. (D and E) The impact of miRNA-144-3p on neurological dysfunction at 1 w post-ICH induction and the brain water content, which was estimated based on five sections per sample. Sham mean values were normalized to 1.0 and all data are displayed as a mean ± SEM ($n = 6$). *P < 0.05 and **P < 0.01 vs. sham group; $^{\#}$P < 0.05, $^{\#\#}$P < 0.01, $^{@}$P < 0.05, $^{@@}$P < 0.01, $^{\$}$P < 0.05, and $^{\$\$}$P < 0.01 vs. their corresponding negative control group, as indicated in the figure. (D) The neurological deficiencies were evaluated based on the criteria of Garcia assessments, $n = 12$. The data are shown as a median with an interquartile range, $n = 12$. *P < 0.05 and **P < 0.01 vs. the sham group; $^{\#}$P < 0.05, $^{\#\#}$P < 0.01, $^{@}$P < 0.05, $^{@@}$P < 0.01, $^{\$}$P < 0.05, $^{\$\$}$P < 0.01 vs. their corresponding negative control group.

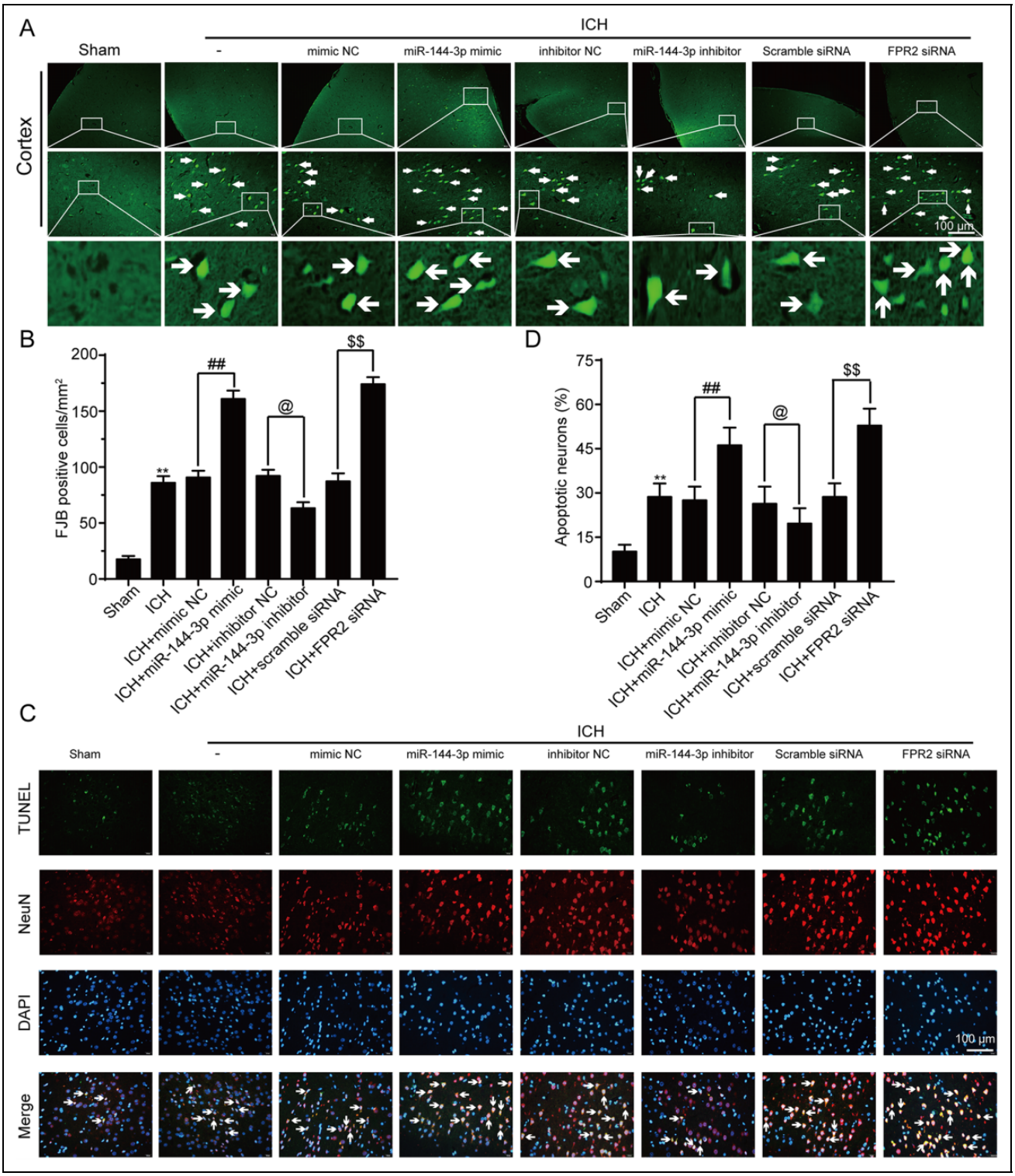

Fig. 4. MiRNA-144-3p induced neuronal death and degradation after ICH. (A) Fluoro-Jade B (FJB) staining of paraffin sections, with arrows indicating FJB-positive cells. (B) The quantification of FJB-positive cells per mm^2. (C) TUNEL staining (green), with neurons strained with NeuN (red). Arrows indicate apoptotic neurons that are NeuN/TUNEL-positive cells. (D) Quantification of TUNEL-positive neuronal cells. In (B) and (D) data are shown as a mean $\pm$ SEM, $n = 6$. *P < 0.05 and **P < 0.01 vs. sham group; ##P < 0.01, @P < 0.05, $$P < 0.01 vs. their corresponding negative control group.

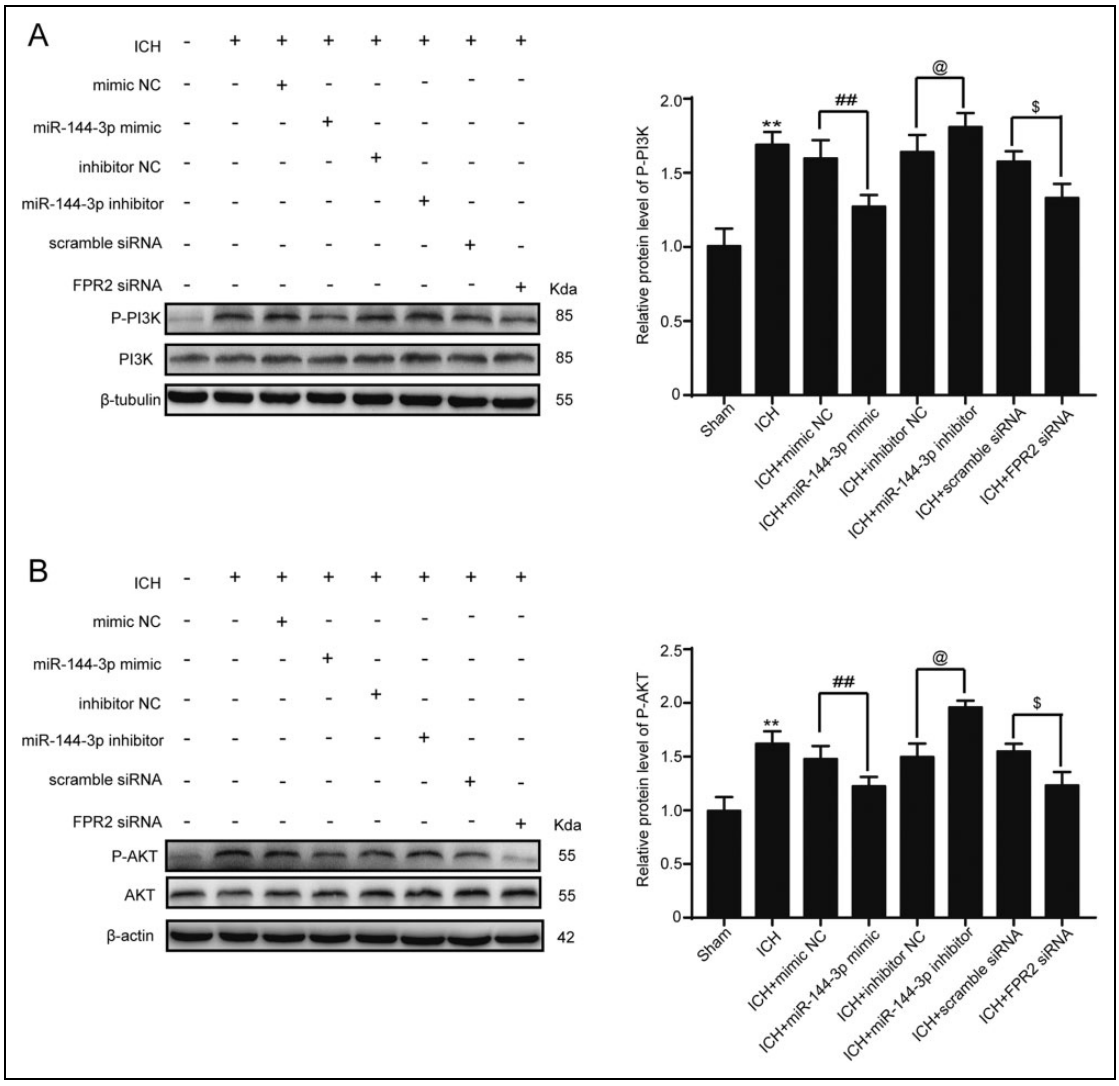

Fig. 5. The effects of miRNA-144-3p and FPR2 on the PI3K/AKT signal pathway *in vivo*. (A and B) Western blot analysis of PI3 K, p-PI3 K, AKT, and p-AKT in brain tissue collected in proximity to the hematoma after being transfected with miRNA-144-3p and FPR2 siRNA. Data are shown as mean ± SEM, $n = 6$. $^{**}P < 0.01$ vs. sham group, $^{\#\#}P < 0.01$, $^{@}P < 0.05$, and $^{\$}P < 0.05$.

the protective effect is associated with the PI3K/AKT signal transduction pathway[22]. To examine the role of this pathway in ICH, we measured p-PI3 K and p-AKT levels in each of the groups after ICH induction. The results showed that in the presence of the miRNA-144-3p mimic, both p-PI3 K and p-AKT were inhibited; however, in the presence of the inhibitor, p-PI3 K and p-AKT were partially elevated relative to the negative control. We did not find prominent changes in total PI3 K or AKT levels in these groups (Figs. 5A and 5B).

Elevated miRNA-144-3p Induces Neuronal Apoptosis by Inhibiting the PI3K/AKT Pathway After OxyHb Treatment In Vitro

To further characterize the interactions between miRNA-144-3p and FPR2, we repeated a similar procedure *in vitro*. First, we exposed neurons to miRNA-144-3p mimics or inhibitor or FPR2 siRNA before adding OxyHb *in vitro*. We then collected the cells for Western blot analysis and examined FPR2 protein levels. The results showed that FPR2 expression decreased after OxyHb treatment when compared with the control group (Fig. 6A), with the lowest point reached much earlier than in the *in vivo* experiment, possibly because of the different environmental conditions. Furthermore, the addition of the miRNA-144-3p mimic only further reduced the FPR2 levels, whereas the miRNA-144-3p inhibitor promoted FPR2 expression (Fig. 6B). To further characterize the impact of OxyHb, flow cytometry was performed to detect neuronal cell apoptosis. Following OxyHb treatment, early-stage apoptotic cell numbers were increased, which was alleviated following miRNA-144-3p inhibitor treatment. Treatment with the miRNA-144-3p mimics, however, increased the number of apoptotic neurons (Fig. 6C).

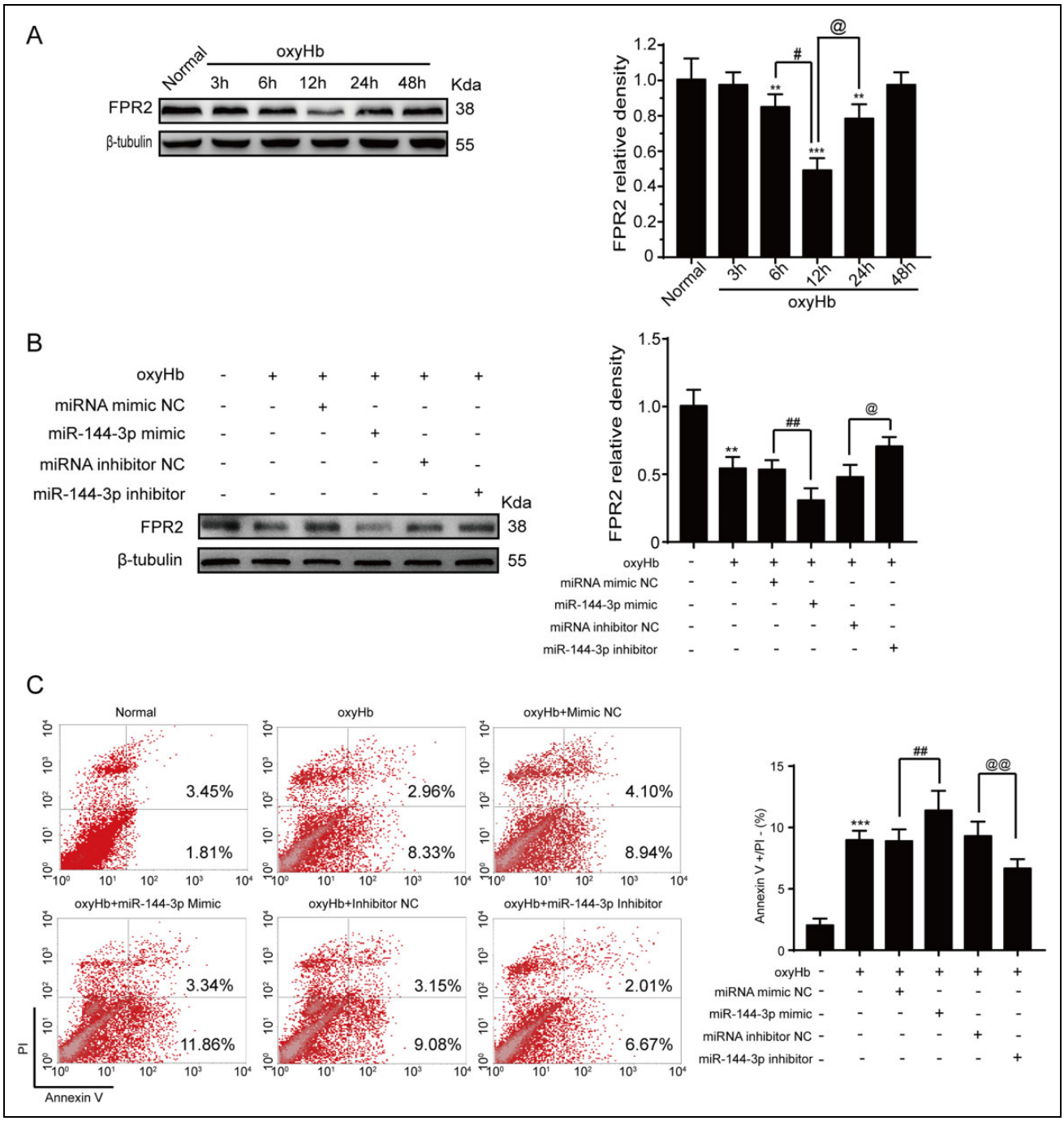

Fig. 6. The effect of miRNA-144-3p on OxyHb-induced ICH in neurons. Primary neurons were cultured and stimulated with 10 μM OxyHb. (A) Western blot analysis examining FPR2 expression levels in neurons treated by OxyHb at the indicated time points. Data are shown as mean ± SEM, $n = 3$. *P < 0.05 and **P < 0.01 vs. control group; #P < 0.05 and @P < 0.05 vs. 12 h. (B) Neurons were transfected with siRNA or plasmid and then stimulated with 10 μM OxyHb for 12 h. The control group was normalized to 1.0 and β-tubulin was used as a loading control. The data are displayed as a mean ± SEM ($n = 3$). **P < 0.01 vs. control group; ##P < 0.01, control group vs. miRNA-144-3p mimic group; and @P < 0.05, control group vs. miRNA-144-3p inhibitor group. (C) The apoptotic neurons were analyzed by flow cytometry, and the apoptotic index was quantified. The data are shown as a mean ± SEM ($n = 3$). **P < 0.01 vs. control group; ##P < 0.01, control group vs. miRNA-144-3p mimic group; and @@P < 0.01, control group vs. miRNA-144-3p inhibitor group.

To further determine the potential impact of miRNA-144-3p on PI3K/AKT signaling following ICH induction, we performed Western blot analysis, which showed similar results to those obtained from the *in vivo* experiment (Figs. 7A and 7B). Previous studies have shown that caspase-3, a downstream factor in the PI3K/AKT pathway,

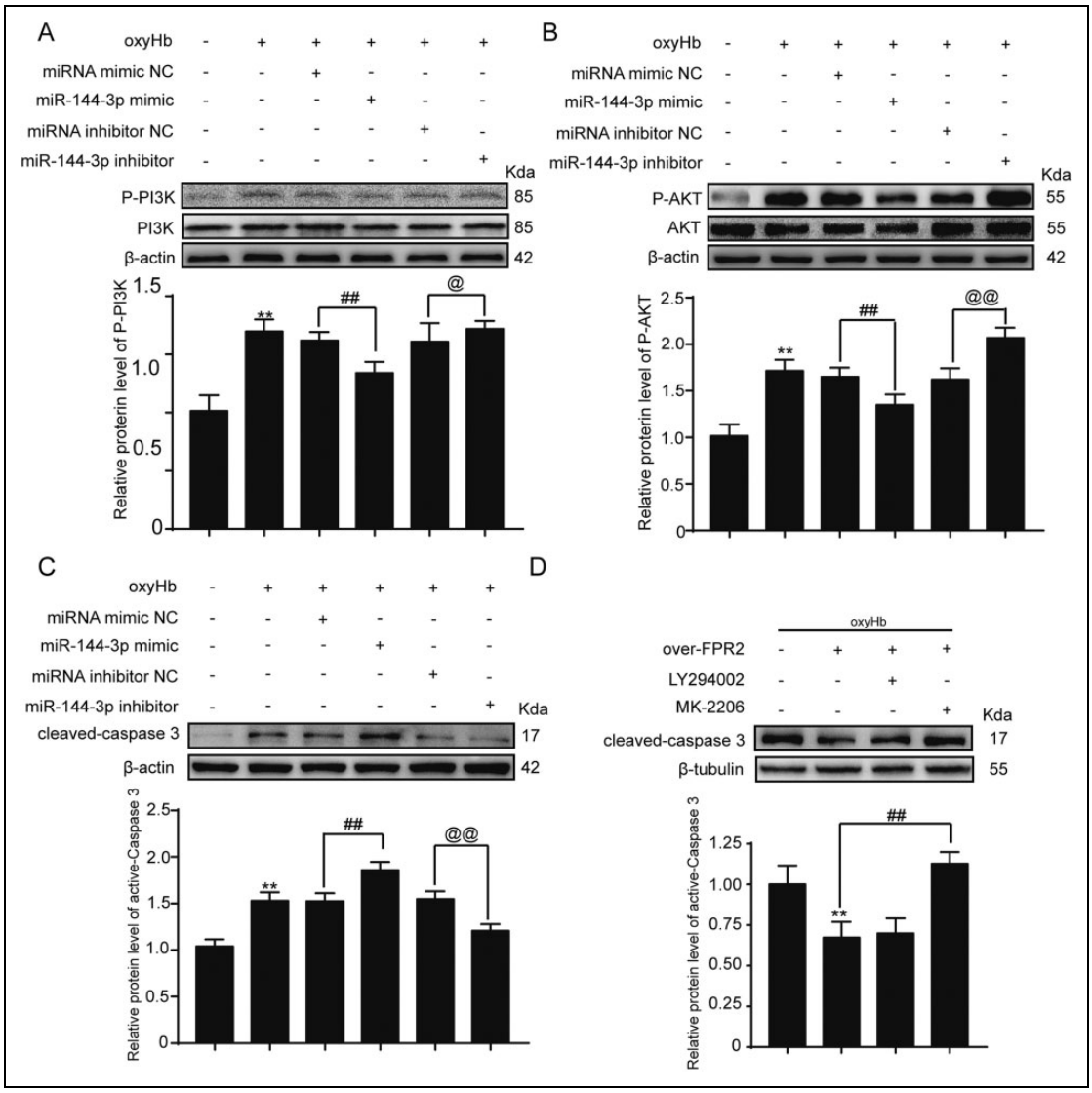

Fig. 7. The effects of miRNA-144-3p and FPR2 on the PI3K/AKT signaling pathway *in vitro*. Neurons were transfected with siRNA or plasmid, and then stimulated with 10 μM OxyHb for 12 h. The cells were then collected and lysed for Western blot analysis. (A) Quantification of PI3K and p-PI3K levels, with p-PI3K levels in the control group normalized to 1.0, while the others were normalized to PI3K. Data are shown as mean ± SEM ($n = 3$). **P < 0.01 vs. control group; ##P < 0.01, control group vs. miRNA-144-3p mimic group; and @P < 0.05, control group vs. miRNA-144-3p inhibitor group. (B) Quantification of AKT and p-AKT, with p-AKT levels in the control group normalized to 1.0, while the others were normalized to AKT. Data are shown as mean ± SEM ($n = 3$). **P < 0.01 vs. control group; ##P < 0.01, control group vs. miRNA-144-3p mimic group; and @@P < 0.01, control group vs. miRNA-144-3p inhibitor group. (C) Quantification of cleaved caspase-3, with protein level in the control group normalized to 1.0 and β-actin used as a loading control. Data are shown as mean ± SEM ($n = 3$). **P < 0.01 vs. control group; ##P < 0.01, control group vs. miRNA-144-3p mimic group; and @@P < 0.01, control group vs. miRNA-144-3p inhibitor group. (D) Neurons overexpressing FPR2 after OxyHb exposure and PI3K/AKT pathway inhibitor treatment. Cleaved caspase-3 levels were quantified and the data are shown as mean ± SEM ($n = 3$). **P < 0.01 vs. control group; ##P < 0.01, OxyHb group vs. Mk-2206 group.

acts as a terminal shear enzyme during the process of intrinsic apoptosis[39]. In the presence of the miRNA-144-3p mimic, cleaved caspase-3 expression was promoted, while the inhibitor showed an opposite trend (Fig. 7C).

Furthermore, cleaved caspase-3 protein levels were shown to decrease during FPR2 overexpression relative to the OxyHb treatment group. Conversely, caspase-3 activation was exacerbated after OxyHb stimulation when PI3 K and AKT were blocked in advance using LY294002 and MK-2206 inhibitors[40] (Fig 7D).

Discussion

It is well established that in response to ICH, brain tissue reacts by altering the regulation of various processes, such as apoptosis, necroptosis, inflammatory responses, and

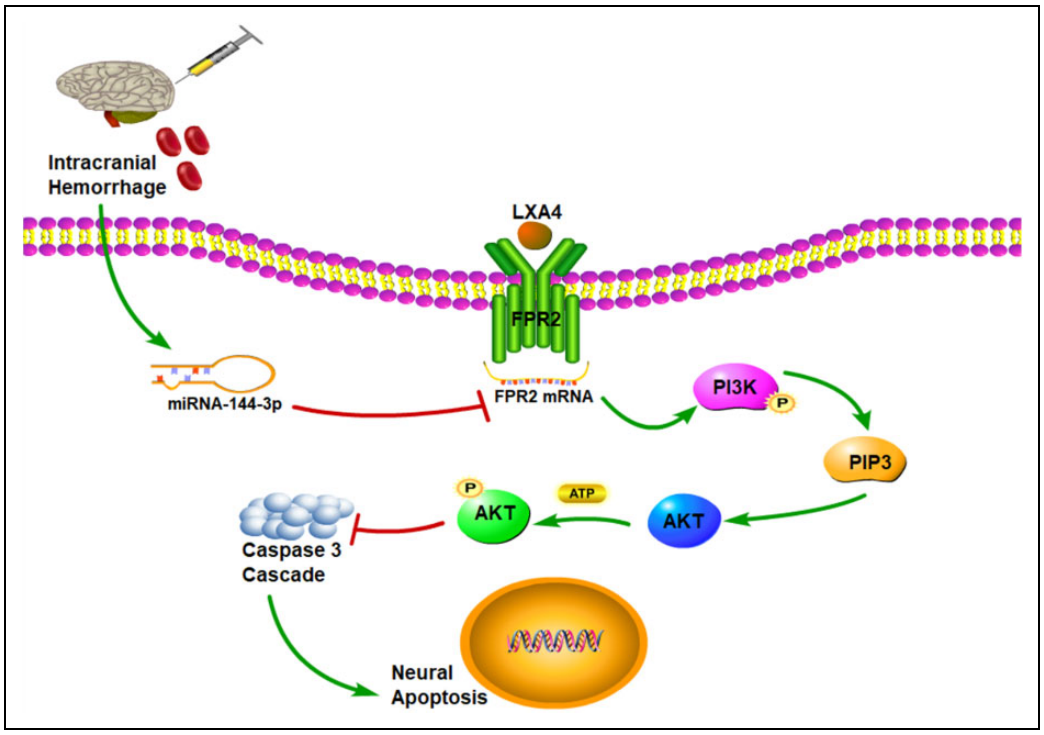

Fig. 8. Illustration of the mechanisms of miRNA-144-3p in ICH-induced SBI. Endogenous miRNA-144-3p is activated after stimulation from blood cells and the hematoma. The miRNA-144-3p then binds the FPR2 3′-UTR and subsequently downregulates its expression at the transcriptional phase. FPR2 exhibits a neural protective function by activating the PI3K/AKT signal pathway, which may subsequently suppress the caspase-3 cascade and inhibit apoptosis.

autophagy. These alterations can subsequently induce accidental cell death or SBI as a result of the aggravate dysfunction and neurological deficiencies[2]. Unfortunately, despite operational improvement techniques and peripheral surgical management, the immediate mortality and long-term prognosis following ICH remain unsatisfactory[8].

Previous studies have shown that miRNA-144-3p can be localized to the nucleus or cytoplasm after various pathological and pharmacological processes, thereby downregulating the activation of the target protein and weakening its corresponding function[32,41]. Moreover, in NSCLC tumors, miRNA-144-3p has been shown to inhibit tumor growth and induce apoptosis[17], while in ICH, miRNA-144 induces microglial autophagy and inflammation[19]. The potential roles of miRNA-144-3p are poorly understood, however, and whether miRNA-144-3p can potentially be a diagnostic biomarker or a therapeutic target should be further investigated.

In this study, miRNA-144-3p expression in the perihematomal region of the brain after ICH induction was higher when compared with the controls. Moreover, after utilizing TargetScan and MicroRNA, we verified the hypothesis that miRNA-144-3p can downregulate FPR2 by binding to its 3′-UTR. However, the relationship between miRNA-144-3p and FPR2 had not yet been defined. Therefore, the main focus was on whether miRNA-144-3p could target FPR2 and what affect miRNA-144-3p has on brain injury after ICH.

FPR2, a formyl peptide receptor, has been identified in multiple cell types and has been found to have diverse functions, such as anti-inflammatory, cell proliferation, inhibiting carcinoma cell invasion, and neural protection[23,42]. Smith et al. described in detail the beneficial role of FPR2 in acute stroke and following ischemia/reperfusion injury[28]. Furthermore, other studies have suggested that FPR2 regulates neutrophil–platelet aggregation and can attenuate cerebral inflammation following ischemia-reperfusion injury, but the role of FPR2 in ICH is poorly characterized[43]. In SAH, one study reported that relative brain FPR2 levels were gradually altered and peaked at 24 h post-induction[22]. In contrast, this study found that FPR2 levels were downregulated after ICH induction. This difference may be attributed to the fact that while both conditions have cerebral bleeding in common, they have quite different etiologies and pathologies. Additionally, the brain tissue samples were extracted from the disparate region in that study. Moreover, because ICH occurs at the basal ganglia, it could possibly generate mechanical injury because of the hematoma mass, whereas in SAH, the blood is disseminated; thus, ICH has been associated with accidental cell death[44]. To further examine the impact of miRNA-144-3p on FPR2 after ICH induction, we biologically synthesized and examined an miRNA-144-3p mimic and inhibitor both *in vivo* and *in vitro*. The results showed that when miRNA-144-3p is upregulated, FPR2 expression is significantly downregulated. Moreover, in the

presence of the miRNA-144-3p inhibitor, neurological scores and brain edema were improved, whereas the mimic had the opposite effect. These findings suggest that miRNA-144-3p downregulates FPR2 expression by suppressing its activation and transduction, thereby inhibiting neural protection and aggravating the brain injury.

To determine the molecular mechanisms governing FPR2 in ICH, other signaling pathways shown to interact with FPR2 were also considered[30]. In one study examining mouse stem cell neural differentiation, formyl peptide receptors were found to be promoted via the PI3K/AKT pathway[29]. Furthermore, other studies have shown that PI3K/AKT signaling is involved in the process of cerebral hemorrhage and induces neural protection[19,40,45,46]. To further investigate this association between FPR2 and the PI3K/AKT pathway, we inhibited p-PI3 K and p-AKT in combination with FPR2 overexpression. The results showed that FPR2 exhibits its neuroprotective effects through the activation of the PI3K/AKT signaling pathway during ICH.

However, miRNA-144-3p is not a unique upstream modulator. In our previous study, annexin A1 phosphorylation was shown to affect anti-necroptosis after ICH induction by combining with the FPR2 receptor[47]. One limitation of the present study was that only young male rats were utilized and females or old ones were not considered. Additionally, this study focused only on neurons, and thus further investigation into interactions between miRNA-144-3p and FPR2 should be performed in microglia, astrocyte, oligodendrocyte, and epithelial cells.

Conclusions

In conclusion, this study showed that in response to ICH, miRNA-144-3p expression was increased and subsequently targeted FPR2, thereby lowering its expression and contributing to neuron apoptosis and brain injury. These findings suggest that miRNA-144-3p may be a potential biomarker for ICH prognosis and that FPR2 may be a potential therapeutic target for ICH-induced SBI.

Authors' Contributions

GC and YL conceived and designed the study, including quality assurance and control. WF, XL, and DZ carried out the experiments. HL and HS prepared the "Methods and Materials" section of the text and performed the statistical analysis. WF and XL helped to draft the manuscript. All authors read and approved the final manuscript.

Weijian Fan and Xiang Li contributed equally to this work.

Abbreviations

FPR2, formyl peptide receptor 2; ICH, intracranial hemorrhage; PI3K, phosphoinositide 3-kinase; AVM, arteriovenous malformations; SBI, secondary brain injury; UTR, untranslated region; LXA4, lipoxin A4; SAH, subarachnoid hemorrhage; CSF, cerebrospinal fluid.

Ethics Approval and Consent to Participate

All management procedures were approved by the Suzhou University Animal Protection Committee and were conducted in accordance with the National Institutes of Health's guidelines on the care and use of animals. All animal research data were written according to ARRIVE (Animal Research: Reporting *In Vivo* Experiments) guidelines.

Statement of Informed Consent

There are no human subjects in this article and informed consent is not applicable.

Statement of Human and Animal Rights

We tried our best to minimize the use of animals and reduce their pain.

Declaration of Conflicting Interests

The authors declared no potential conflicts of interest with respect to the research, authorship, and/or publication of this article.

Funding

The authors disclosed receipt of the following financial support for the research, authorship, and/or publication of this article: This work was supported by the Project of Jiangsu Provincial Medical Innovation Team (No. CXTDA2017003), Jiangsu Provincial Medical Youth Talent (No. QNRC2016728), Natural Science Foundation of Jiangsu Province (BK20180204), the National Key R&D Program of China (No. 2018YFC1312600 & No. 2018YFC1312601), Suzhou Key Medical Centre (No. Szzx201501), Scientific Department of Jiangsu Province (No. BE2017656), and Suzhou Government (LCZX201601).

References

1. Mendelow AD, Gregson BA, Rowan EN, Murray GD, Gholkar A, Mitchell PM, Investigators SI. Early surgery versus initial conservative treatment in patients with spontaneous supratentorial lobar intracerebral haematomas (STICH II): a randomised trial. Lancet. 2013;382(9890):397–408.
2. Schlunk F, Greenberg SM. The pathophysiology of intracerebral hemorrhage formation and expansion. Transl Stroke Res. 2015;6(4):257–263.
3. Lapchak PA, Zhang JH. The high cost of stroke and stroke cytoprotection research. Transl Stroke Res. 2017;8(4): 307–317.
4. Jiang B, Li L, Chen Q, Tao Y, Yang L, Zhang B, Zhang JH, Feng H, Chen Z, Tang J, Zhu G. Role of glibenclamide in brain injury after intracerebral hemorrhage. Transl Stroke Res. 2017; 8(2):183–193.
5. Gao L, Xu W, Li T, Chen J, Shao A, Yan F, Chen G. Stem cell therapy: a promising therapeutic method for intracerebral hemorrhage. Cell Transplant. 2018;27(12):1809–1824.
6. Ahn SY, Chang YS, Sung DK, Sung SI, Ahn JY, Park WS. Pivotal role of brain-derived neurotrophic factor secreted by mesenchymal stem cells in severe intraventricular hemorrhage in newborn rats. Cell Transplant. 2017;26(1):145–156.
7. Joseph MJ, Caliaperumal J, Schlichter LC. After intracerebral hemorrhage, oligodendrocyte precursors proliferate and

differentiate inside white-matter tracts in the rat striatum. Transl Stroke Res. 2016;7(3):192–208.
8. Chen S, Yang Q, Chen G, Zhang JH. An update on inflammation in the acute phase of intracerebral hemorrhage. Transl Stroke Res. 2015;6(1):4–8.
9. Felekkis K, Touvana E, Stefanou C, Deltas C. microRNAs: a newly described class of encoded molecules that play a role in health and disease. Hippokratia. 2010;14(4):236–240.
10. Liu H, Lei C, He Q, Pan Z, Xiao D, Tao Y. Nuclear functions of mammalian microRNAs in gene regulation, immunity and cancer. Mol Cancer. 2018;17(1):64.
11. Xu W, Gao L, Zheng J, Li T, Shao A, Reis C, Chen S, Zhang J. The roles of microRNAs in stroke: possible therapeutic targets. Cell Transplant. 2018;27(12):1778–1788.
12. Yu W, Huang X, Tian X, Zhang H, He L, Wang Y, Nie Y, Hu S, Lin Z, Zhou B, Pu W, Lui KO, Zhou B. GATA4 regulates Fgf16 to promote heart repair after injury. Development. 2016; 143(6):936–949.
13. Guan H, Liang W, Xie Z, Li H, Liu J, Liu L, Xiu L, Li Y. Down-regulation of miR-144 promotes thyroid cancer cell invasion by targeting ZEB1 and ZEB2. Endocrine. 2015; 48(2):566–574.
14. Xiao W, Lou N, Ruan H, Bao L, Xiong Z, Yuan C, Tong J, Xu G, Zhou Y, Qu Y, Hu W, Gao Y, Ru Z, Liu L, Xiao H, Chen K, Yang H, Zhang X. Mir-144-3p promotes cell proliferation, metastasis, sunitinib resistance in clear cell renal cell carcinoma by downregulating ARID1A. Cell Physiol Biochem. 2017;43(6):2420–2433.
15. Wu M, Huang C, Huang X, Liang R, Feng Y, Luo X. MicroRNA-144-3p suppresses tumor growth and angiogenesis by targeting SGK3 in hepatocellular carcinoma. Oncol Rep. 2017;38(4):2173–2181.
16. Zhao Y, Xie Z, Lin J, Liu P. MiR-144-3p inhibits cell proliferation and induces apoptosis in multiple myeloma by targeting c-Met. Am J Transl Res. 2017;9(5):2437–2446.
17. Zha W, Cao L, Shen Y, Huang M. Roles of Mir-144-ZFX pathway in growth regulation of non-small-cell lung cancer. Plos One. 2013;8(9):e74175.
18. Liu F, Wang J, Fu Q, Zhang X, Wang Y, Liu J, Huang J, Lv X. VEGF-activated miR-144 regulates autophagic survival of prostate cancer cells against cisplatin. Tumour Biol. 2015; 37(12):15627–15633.
19. Zhao Y, Wei ZZ, Zhang JY, Zhang Y, Won S, Sun J, Yu SP, Li J, Wei L. GSK-3beta inhibition induced neuroprotection, regeneration, and functional recovery after intracerebral hemorrhagic stroke. Cell Transplant. 2017;26(3):395–407.
20. Li Y, Zhao Y, Cheng M, Qiao Y, Wang Y, Xiong W, Yue W. Suppression of microRNA-144-3p attenuates oxygen–glucose deprivation/reoxygenation-induced neuronal injury by promoting Brg1/Nrf2/ARE signaling. J Biochem Mol Toxicol. 2018; 32(4):e22044.
21. Wang P, Liang X, Lu Y, Zhao X, Liang J. MicroRNA-93 downregulation ameliorates cerebral ischemic injury through the Nrf2/HO-1 defense pathway. Neurochem Res. 2016; 41(10):2627–2635.
22. Guo Z, Hu Q, Xu L, Guo ZN, Ou Y, He Y, Yin C, Sun X, Tang J, Zhang JH. Lipoxin A4 reduces inflammation through formyl peptide receptor 2/p38 MAPK signaling pathway in subarachnoid hemorrhage rats. Stroke. 2016;47(2):490–497.
23. Ke Y, Zebda N, Oskolkova O, Afonyushkin T, Berdyshev E, Tian Y, Meng F, Sarich N, Bochkov VN, Wang JM, Birukova AA, Birukov KG. Anti-inflammatory effects of OxPAPC involve endothelial cell-mediated generation of LXA4. Circ Res. 2017;121(3):244–257.
24. Serhan CN, Chiang N. Endogenous pro-resolving and anti-inflammatory lipid mediators: a new pharmacologic genus. Br J Pharmacol. 2008;153(suppl 1):S200–S215.
25. Chiang N, Serhan CN, Dahlen SE, Drazen JM, Hay DW, Rovati GE, Shimizu T, Yokomizo T, Brink C. The lipoxin receptor ALX: potent ligand-specific and stereoselective actions in vivo. Pharmacol Rev. 2006;58(3):463–487.
26. Cao Y, Ye Q, Zhuang M, Xie S, Zhong R, Cui J, Zhou J, Zhu Y, Zhang T, Cao L. Ginsenoside Rg3 inhibits angiogenesis in a rat model of endometriosis through the VEGFR-2-mediated PI3K/Akt/mTOR signaling pathway. Plos One. 2017;12(11):e0186520.
27. Su LD, Peng JM, Ge YB. Formyl peptide receptor 2 mediated chemotherapeutics drug resistance in colon cancer cells. Eur Rev Med Pharmacol Sci. 2018;22(1):95–100.
28. Smith HK, Gil CD, Oliani SM, Gavins FN. Targeting formyl peptide receptor 2 reduces leukocyte–endothelial interactions in a murine model of stroke. FASEB J. 2015;29(5): 2161–2171.
29. Zhang L, Wang G, Chen X, Xue X, Guo Q, Liu M, Zhao J. Formyl peptide receptors promotes neural differentiation in mouse neural stem cells by ROS generation and regulation of PI3K–AKT signaling. Sci Rep. 2017;7(1):206.
30. Cattaneo F, Parisi M, Ammendola R. Distinct signaling cascades elicited by different formyl peptide receptor 2 (FPR2) agonists. Int J Mol Sci. 2013;14(4):7193–7230.
31. Livak KJ, Schmittgen TD. Analysis of relative gene expression data using real-time quantitative PCR and the 2(-delta delta C(T)) method. Methods. 2001;25(4):402–408.
32. Huo F, Zhang C, He H, Wang Y. MicroRNA-144-3p inhibits proliferation and induces apoptosis of human salivary adenoid carcinoma cells via targeting of mTOR. Biotechnol Lett. 2016; 38(3):409–416.
33. Shen H, Chen Z, Wang Y, Gao A, Li H, Cui Y, Zhang L, Xu X, Wang Z, Chen G. Role of neurexin-1beta and neuroligin-1 in cognitive dysfunction after subarachnoid hemorrhage in rats. Stroke. 2015;46(9):2607–2615.
34. Hu Q, Chen C, Yan J, Yang X, Shi X, Zhao J, Lei J, Yang L, Wang K, Chen L, Huang H, Han J, Zhang JH, Zhou C. Therapeutic application of gene silencing MMP-9 in a middle cerebral artery occlusion-induced focal ischemia rat model. Exp Neurol. 2009;216(1):35–46.
35. Garcia JH, Wagner S, Liu KF, Hu XJ. Neurological deficit and extent of neuronal necrosis attributable to middle cerebral artery occlusion in rats. Statistical validation. Stroke. 1995; 26(4):627–634; discussion 635.
36. Dang B, Li H, Xu X, Shen H, Wang Y, Gao A, He W, Wang Z, Chen G. Cyclophilin A/cluster of differentiation 147

interactions participate in early brain injury after subarachnoid hemorrhage in rats. Crit Care Med. 2015;43(9):e369–e381.
37. Senn C, Hangartner C, Moes S, Guerini D, Hofbauer KG. Central administration of small interfering RNAs in rats: a comparison with antisense oligonucleotides. Eur J Pharmacol. 2005;522(1–3):30–37.
38. Wang Z, Zhou F, Dou Y, Tian X, Liu C, Li H, Shen H, Chen G. Melatonin alleviates intracerebral hemorrhage-induced secondary brain injury in rats via suppressing apoptosis, inflammation, oxidative stress, DNA damage, and mitochondria injury. Transl Stroke Res. 2018;9(1):74–91.
39. Han BH, DeMattos RB, Dugan LL, Kim-Han JS, Brendza RP, Fryer JD, Kierson M, Cirrito J, Quick K, Harmony JA, Aronow BJ, Holtzman DM. Clusterin contributes to caspase-3-independent brain injury following neonatal hypoxia-ischemia. Nat Med. 2001;7(3):338–343.
40. Ma J, Wang Z, Liu C, Shen H, Chen Z, Yin J, Zuo G, Duan X, Li H, Chen G. Pramipexole-induced hypothermia reduces early brain injury via PI3K/AKT/GSK3beta pathway in subarachnoid hemorrhage rats. Sci Rep. 2016; 6:23817.
41. Guo L, Zhou L, Gao Q, Zhang A, Wei J, Hong D, Chu Y, Duan X, Zhang Y, Xu G. MicroRNA-144-3p inhibits autophagy activation and enhances Bacillus Calmette-Guerin infection by targeting ATG4a in RAW264.7 macrophage cells. Plos One. 2017;12(6):e0179772.
42. Butcher MJ, Galkina EV. wRAPping up early monocyte and neutrophil recruitment in atherogenesis via annexin A1/FPR2 signaling. Circ Res. 2015;116(5):774–777.
43. Vital SA, Becker F, Holloway PM, Russell J, Perretti M, Granger DN, Gavins FN. Formyl-peptide receptor 2/3/lipoxin A4 receptor regulates neutrophil–platelet aggregation and attenuates cerebral inflammation: impact for therapy in cardiovascular disease. Circulation. 2016;133(22):2169–2179.
44. Darzynkiewicz Z, Juan G, Li X, Gorczyca W, Murakami T, Traganos F. Cytometry in cell necrobiology: analysis of apoptosis and accidental cell death (necrosis). Cytometry. 1997; 27(1):1–20.
45. Cui J, Cui C, Cui Y, Li R, Sheng H, Jiang X, Tian Y, Wang K, Gao J. Bone marrow mesenchymal stem cell transplantation increases GAP-43 expression via ERK1/2 and PI3K/Akt pathways in intracerebral hemorrhage. Cell Physiol Biochem. 2017;42(1):137–144.
46. Yang D, Han Y, Zhang J, Chopp M, Seyfried DM. Statins enhance expression of growth factors and activate the PI3K/Akt-mediated signaling pathway after experimental intracerebral hemorrhage. World J Neurosci. 2012;2(2):74–80.
47. Wang Z, Chen Z, Yang J, Yang Z, Yin J, Zuo G, Duan X, Shen H, Li H, Chen G. Identification of two phosphorylation sites essential for annexin A1 in blood–brain barrier protection after experimental intracerebral hemorrhage in rats. J Cereb Blood Flow Metab. 2017;37(7):2509–2525.